Record-setting algal bloom in Lake Erie caused by agricultural and meteorological trends consistent with expected future conditions

Anna M. Michalak[a,1], Eric J. Anderson[b], Dmitry Beletsky[c], Steven Boland[d], Nathan S. Bosch[e], Thomas B. Bridgeman[f], Justin D. Chaffin[f], Kyunghwa Cho[g,2], Rem Confesor[h], Irem Daloğlu[g], Joseph V. DePinto[i], Mary Anne Evans[g,3], Gary L. Fahnenstiel[j], Lingli He[k], Jeff C. Ho[l], Liza Jenkins[g,j], Thomas H. Johengen[c], Kevin C. Kuo[d,m], Elizabeth LaPorte[n], Xiaojian Liu[d], Michael R. McWilliams[o], Michael R. Moore[g], Derek J. Posselt[d], R. Peter Richards[h], Donald Scavia[g], Allison L. Steiner[d], Ed Verhamme[i], David M. Wright[d], and Melissa A. Zagorski[d]

[a]Department of Global Ecology, Carnegie Institution for Science, Stanford, CA 94305; [b]Great Lakes Environmental Research Laboratory, National Oceanic and Atmospheric Administration, Ann Arbor, MI 48108; [c]Cooperative Institute for Limnology and Ecosystems Research, School of Natural Resources and Environment, University of Michigan, Ann Arbor, MI 48109; [d]Department of Atmospheric, Oceanic and Space Sciences, University of Michigan, Ann Arbor, MI 48109; [e]Environmental Science, Grace College, Winona Lake, IN 46590; [f]Department of Environmental Sciences, University of Toledo, Toledo, OH 43606 [g]School of Natural Resources and Environment, University of Michigan, Ann Arbor, MI 48109; [h]National Center for Water Quality Research, Heidelberg University, Tiffin, OH 44883; [i]LimnoTech, Ann Arbor, MI 48108; [j]Michigan Tech Research Institute, Michigan Technological University, Ann Arbor, MI 48105; [k]Department of Civil and Environmental Engineering, University of Michigan, Ann Arbor, MI 48109; [l]Department of Civil and Environmental Engineering, Stanford University, Stanford, CA 94305; [m]School of Public Policy, University of Michigan, Ann Arbor, MI 48109; [n]Michigan Sea Grant, School of Natural Resources and Environment, University of Michigan, Ann Arbor, MI 48104; and [o]Department of Economics, University of Michigan, Ann Arbor, MI 48109

Edited by Robert E. Hecky, University of Minnesota, Duluth, MN, and accepted by the Editorial Board March 4, 2013 (received for review September 27, 2012)

In 2011, Lake Erie experienced the largest harmful algal bloom in its recorded history, with a peak intensity over three times greater than any previously observed bloom. Here we show that long-term trends in agricultural practices are consistent with increasing phosphorus loading to the western basin of the lake, and that these trends, coupled with meteorological conditions in spring 2011, produced record-breaking nutrient loads. An extended period of weak lake circulation then led to abnormally long residence times that incubated the bloom, and warm and quiescent conditions after bloom onset allowed algae to remain near the top of the water column and prevented flushing of nutrients from the system. We further find that all of these factors are consistent with expected future conditions. If a scientifically guided management plan to mitigate these impacts is not implemented, we can therefore expect this bloom to be a harbinger of future blooms in Lake Erie.

extreme precipitation events | climate change | aquatic ecology | *Microcystis* sp. | *Anabaena* sp.

Eutrophication of freshwater and coastal marine ecosystems resulting from increased anthropogenic nutrient loading to receiving waters has become a global problem (1). Examples of eutrophic lakes with severe toxic cyanobacterial blooms include Lake Taihu in China (2), Lake Winnipeg in Canada (3), and Lake Nieuwe Meer in The Netherlands (4). Lake Erie, the shallowest, most productive, and most southern of the Laurentian Great Lakes, has experienced substantial eutrophication over the past half century. In the 1960s and 1970s, excess phosphorus from point and nonpoint sources produced nuisance algal blooms, poor water clarity, and extensive hypoxic areas (5). In response, the United States and Canada implemented phosphorus loading reduction strategies through the Great Lakes Water Quality Agreement (6, 7). These load reductions resulted in a rapid and profound ecological response as predicted by a range of models (8–10). Despite early success from these management actions, however, hypolimnetic oxygen depletion rates, hypoxia extent (11, 12), and algal biomass (13–15) have increased systematically since the mid-1990s. Of greatest concern is the increase in toxin-forming strains of the cyanobacteria *Microcystis* sp. and *Anabaena* sp. that produce the hepatotoxin microcystin and the neurotoxin anatoxin, respectively. Even nontoxic forms of these blooms, however, severely stress the ecological structure and functioning, as well as the aesthetics, of the Lake Erie ecosystem. Possible causes for these more recent increases include increases in agricultural nonpoint sources of bioavailable phosphorus (16), the presence of invasive mussel species, specifically *Dreissena rostriformis bugensis* (quagga mussels) and *Dreissenid polymorpha* (zebra mussels) (17–20), and internal phosphorus loading to Lake Erie's central basin that increases in response to hypoxic conditions (21).

In 2011, Lake Erie experienced an algal bloom of record-setting magnitude (Fig. 1). Land use, agricultural practices, and meteorological conditions may all have contributed to stimulating and exacerbating the bloom. We hypothesize that severe spring precipitation events, coupled with long-term trends in agricultural land use and practices, produced a pulse of remarkably high loading of highly bioavailable dissolved reactive phosphorus (DRP) to the western basin of Lake Erie. Uncommonly warm and quiescent conditions in late spring and summer, and an unusually strong resuspension event immediately preceding bloom onset, are further hypothesized to have provided ideal incubation, seeding, and growth conditions for bloom development. *Dreissenid* populations (22, 23), and phosphorus levels in lake sediments (24, 25) have been stable in recent years, and neither of these factors is therefore hypothesized to be a significant additional contributing factor. Here we test these causal hypotheses and their correspondence with long-

Author contributions: A.M.M., E.J.A., D.B., N.S.B., T.B.B., R.C., J.V.D., J.C.H., M. R. Moore, D.J.P., R.P.R., D.S., and A.L.S. designed research; A.M.M., E.J.A., D.B., S.B., N.S.B., T.B.B., J.D.C., K.C., R.C., I.D., M.A.E., G.L.F., L.H., J.C.H., L.J., T.H.J., K.C.K., X.L., M. R. McWilliams, M. R. Moore, D.J.P., R.P.R., D.S., A.L.S., D.M.W., and M.A.Z. performed research; A.M.M., E.J.A., D.B., S.B., N.S.B., T.B.B., J.D.C., K.C., R.C., I.D., J.V.D., M.A.E., L.H., J.C.H., L.J., T.H.J., K.C.K., X.L., M. R. McWilliams, M. R. Moore, D.J.P., R.P.R., D.S., A.L.S., E.V., D.M.W., and M.A.Z. analyzed data; and A.M.M., E.J.A., D.B., N.S.B., T.B.B., J.D.C., K.C., I.D., J.V.D., M.A.E., J.C.H., T.H.J., E.L., M. R. McWilliams, M. R. Moore, D.J.P., R.P.R., D.S., and A.L.S. wrote the paper.

The authors declare no conflict of interest.

This article is a PNAS Direct Submission. R.E.H. is a guest editor invited by the Editorial Board.

Freely available online through the PNAS open access option.

[1]To whom correspondence should be addressed. E-mail: michalak@stanford.edu.

[2]Present address: School of Urban and Environmental Engineering, Ulsan National Institute of Science and Technology, Ulsan 689-798, Republic of Korea.

[3]Present address: US Geological Survey, Great Lakes Science Center, Ann Arbor, MI 48105.

This article contains supporting information online at www.pnas.org/lookup/suppl/doi:10.1073/pnas.1216006110/-/DCSupplemental.

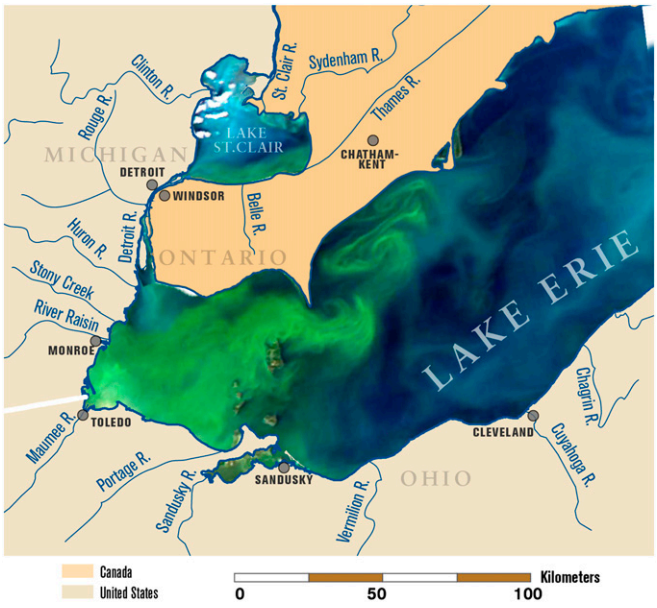

Fig. 1. MODIS satellite Image of Lake Erie on September 3, 2011, overlaid over map of Lake Erie tributaries. This image shows the bloom about 6 wk after its initiation in the western basin. On this date, it covers the entire western basin and is beginning to expand into the central basin, where it will continue to grow until October (Fig. S1).

term trends to assess whether the 2011 bloom was driven by a unique and unfortunate combination of circumstances or whether it is a harbinger of future eutrophication conditions expected under evolving land management practices and climate change in the region.

Results and Discussion

Lake Erie's 2011 algal bloom began in its western basin in mid-July, and estimates from remotely sensed data (26) indicate that it covered an area of ~600 km^2 during the initial phase (Fig. S1). In situ sampling of algal biovolume, areal coverage, and duration indicate that by early September the bloom was at least 2.4 times greater than the previous largest bloom (2008), and four times greater than the average of blooms between 2002 and 2010 (14). As *Microcystis* declined in the western basin in the latter part of the summer, the bloom spread into the central basin, eventually extending 150 km eastward and persisting until mid-October. At its peak in early October, the extent of the bloom was estimated to be more than 5,000 km^2 (26) (Fig. S1). The peak bloom intensity, calculated from remote sensing, was 7.3 times greater than the average for the previous 9 years and 3.3 times greater than the previous peak observed in 2008. Cyanobacteria, which were undetectable in June, represented 60–98% of in situ fluorescence measured from surface water throughout the western basin during the bloom.

Taxonomic analysis of the phytoplankton community confirmed that composition was almost entirely *Microcystis*. Microcystin toxin was detected at most western basin sampling sites with water-column integrated concentrations ranging from 0.1 μg/L to 8.7 μg/L. Surface toxin concentrations could have reached over 4,500 μg/L in early August assuming all *Microcystis* and microcystin formed a surface scum 10 cm in thickness. The World Health Organization guideline for microcystin in recreational waters is 20 μg/L (27), pointing to potential for adverse health effects in 2011. DNA analysis of *Microcystis* from various locations indicated similar strains in the western and central basins, suggesting that the central basin bloom arose from the eastward migration of *Microcystis* colonies from the original bloom. As the abundance of the nonnitrogen fixing *Microcystis* began to decline significantly in the western basin in late August, it was replaced by a secondary bloom of nitrogen-fixing *Anabaena* sp., suggesting that the *Microcystis* bloom had largely depleted bioavailable nitrogen in the lake. This was confirmed by in situ sampling of algal nutrient concentrations (*SI Materials and Methods* and *SI Results and Discussion*).

Microcystis sp. and *Anabaena* sp. are both potentially toxic cyanobacteria. *Microcystis* thrives in Lake Erie, where its growth is stimulated by high concentrations of DRP and combined inorganic nitrogen (i.e., ammonia and nitrate) (28). Concentrations of bioavailable phosphorus appear to govern the ultimate biomass of *Microcystis*, but Lake Erie's low bioavailable nitrogen-to-phosphorus ratio in late summer also provides cyanobacteria, including those that are nonnitrogen fixing, an additional competitive advantage over other phytoplankton classes (29–31). Temperature and mixing conditions are also important in determining growth, because cyanobacteria have a higher temperature optimum (on the order of 25 °C) than eukaryotic phytoplankton (17, 32), and temperature-dependent gas vacuoles increase *Microcystis* buoyancy, allowing them to rise to more favorable light and temperature conditions under quiescent conditions (33).

We hypothesize that trends in agricultural land use contributed to the 2011 bloom. Corn cropland increased 11% nationally and land in the federal Conservation Reserve Program (CRP) decreased 14% between 2008 and 2011 (Fig. S2). Similar trends in the western Lake Erie watershed could lead to increased phosphate fertilizer use, because phosphate is applied to corn at a 36% higher rate than to soybeans in Ohio (*SI Materials and Methods* and *SI Results and Discussion*), and because the conversion of CRP land to agriculture would also substantially increase phosphate use. Together, these could result in greater phosphorus runoff and higher loadings in western Lake Erie. However, trends in the Lake Erie watershed deviate sharply from those national trends. Both corn cropland and CRP land changed only slightly from 2008 to 2011 (*SI Materials and Methods*, *SI Results and Discussion*, and Fig. S2). It is therefore unlikely that recent agricultural land use trends are important drivers of the 2011 bloom.

Long-term trends in agricultural nutrient management practices, on the other hand, are consistent with a potential for higher nutrient loading (Table S1). Three management practices—autumn fertilizer application, fertilizer being broadcast on the surface rather than injected in the soil, and conservation tillage—can create conditions for enhanced DRP runoff. These practices have increased in the region over the last 10 y, although in some cases evidence is only anecdotal. Consistent with these trends is the observed 218% increase in DRP loadings between 1995 and 2011 ($P = 0.0004$) from the Maumee River, the main tributary to the western basin, whereas runoff increased by only 42% ($P = 0.12$) over the same period (*SI Materials and Methods*, *SI Results and Discussion* and Table S2).

Autumn weather conditions in 2010 were ideal for completing harvest and preparing fields for the following year, increasing autumn application of fertilizer. The spring of 2011 then experienced a series of large storm runoff events between February 17 and June 8, including a major event with peak daily mean discharge exceeding 2,200 m^3/s on May 25–27 (*SI Materials and Methods* and *SI Results and Discussion* and Fig. 2*A*). This storm represents the 99.8th percentile for Maumee daily discharge since 1975, when intensive monitoring of this tributary began. During this peak event, convective cells originated from a low-pressure system centered over the southern Great Plains and propagated to the north and east over a 2-d period (Fig. S3). The peak 24-h accumulated precipitation exceeded 50 mm over the Maumee River basin on May 26, contributing to a total of over 170 mm of rain in May 2011. This is over 75% above the prior 20-y average for May (97 mm averaged over 1986–2005). Total discharge and phosphorus loads for the 111-d (February 17 to

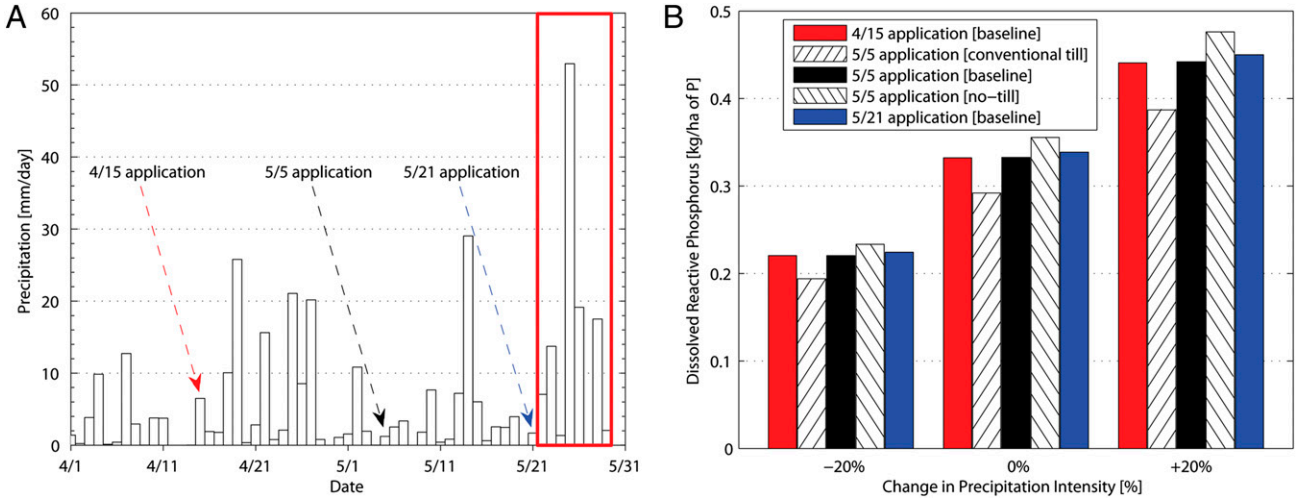

Fig. 2. (*A*) Time series of precipitation over the Maumee watershed, with the three different fertilizer application scenarios (arrows) used in the SWAT simulations. (*B*) Dissolved reactive phosphorus (DRP) yield (kilograms of P per hectares) response to different precipitation intensities, fertilizer application timing, and tillage practices. All DRP yields are summed over May 21–30, 2011 (red box in *A*). Baseline tillage practices include a realistic combination of conventional and no-till practices. Alternate tillage practice scenarios include either all conventional or all no-till practices with fertilizer application on May 5.

June 8) and 15-d (May 25 to June 8) periods covering the springtime precipitation events (Fig. S4) are among the largest observed since 1975, for periods of those lengths. Similarly, total discharge and DRP loads during the March-to-June timeframe, which is the critical period for setting up algal blooms (26), were the largest since intensive monitoring began in 1975. This is in stark contrast to these months in 2012, when discharge from the Maumee was only 20% and DRP loading was 15% of 2011 values.

We use the Soil and Water Assessment Tool (SWAT) model (34, 35) to test the impact of precipitation intensity and agricultural nutrient management practices on expected nutrient loading, to determine whether these factors are likely to be responsible for the loading observed in 2011. SWAT simulations indicate that DRP yields are sensitive to precipitation intensity (higher intensity increasing yields, Fig. 2*B*), fertilizer application timing (proximity to storm events increasing DRP yields, Fig. 2 *A* and *B*), and tillage practices (no-till increasing DRP yields, Fig. 2*B*), with precipitation having the strongest influence and fertilizer timing having the least influence (*SI Materials and Methods* and *SI Results and Discussion*). This supports the hypothesis that the confluence of long-term trends in agricultural nutrient management practices and extreme precipitation events was a strong contributor to the DRP yields that triggered the 2011 bloom.

We also hypothesize that temperature and wind conditions over the lake both before and during the bloom encouraged bloom growth, because warm and quiescent conditions before bloom onset led to minimal flushing of the system and reduced vertical lake mixing that allows *Microcystis* to take advantage of its buoyancy regulation. However, wind and surface water temperature data from the lake buoy indicate a lower frequency of warm and quiescent conditions during the 2011 prebloom period (defined as daily average wind stress $\tau < 0.05$ Pa and temperature $T > 15$ °C) (36) relative to other bloom years (*SI Materials and Methods* and *SI Results and Discussion*). In addition, although a particularly strong wind-driven resuspension event before the bloom onset could encourage fast initial bloom growth, wind conditions that led to the resuspension event immediately preceding bloom onset were not unusual relative to other years. After bloom initiation, on the other hand, conditions were indeed more conducive to bloom growth relative to other years, as quantified by the percent of time under warm and quiescent conditions after bloom onset (62% relative to 35–56% in other years, $P = 0.015$). These buoy-based observations are consistent with satellite-derived lake temperatures that were 3 °C warmer than the 1992–2011 summer climatology and 1 °C warmer than 2010 temperatures (*SI Materials and Methods*, *SI Results and Discussion*, and Fig. S5).

To investigate the role of lake circulation in encouraging the bloom, we apply 3D hydrodynamic and particle transport models (*SI Materials and Methods* and *SI Results and Discussion*). Simulations show that western basin monthly circulation is characterized by a broad west–east flow that exits the basin via three channels (North, Middle, and South), with low current magnitudes correlated with increased residence times (Fig. 3). All simulated years exhibit relatively low-magnitude currents during summer months (May–August), but 2011 had an extended period with weak currents (consistent with weaker winds) from late winter through summer (February–July) (Fig. S6). The residence times in the western basin during this period were 46% and 36% longer than in the previous years (2009 and 2010, respectively). Furthermore, residence times of Maumee River water in June 2011 were 53% longer than in the previous years and 77% longer (>90 d) than the estimated mean hydraulic residence time of the western basin (Fig. S7). Simulations also show that the long residence times were accompanied by a "short circuiting" of Detroit River waters, leading to minimal mixing between the Detroit and Maumee River waters along the western and southern shores of the basin, thus diminishing dilution of nutrient-rich Maumee River waters. Although some mixing occurs near the islands between the western and central basins during April–August, Detroit and Maumee waters primarily leave the western basin through the North and Middle/South Channels, respectively (Fig. S8). Location and timing of bloom initiation is consistent with simulated advection of the elevated late spring Maumee runoff, suggesting that the water mass present at the first stages of the bloom initiation likely originated from the Maumee River close to June 1.

Of the original hypothesized causes of the monumental 2011 bloom, observations and simulations therefore confirm that long-term trends in agricultural practices are consistent with increasing DRP loads delivered to the western basin of Lake Erie, and that meteorological conditions in spring 2011 led to record-breaking nutrient loads to the lake during the late spring. This conclusion is further supported by substantially lower discharge in 2012 leading to lower DRP loading and a weaker bloom (37). Our results further show that weak circulation during summer 2011 led to

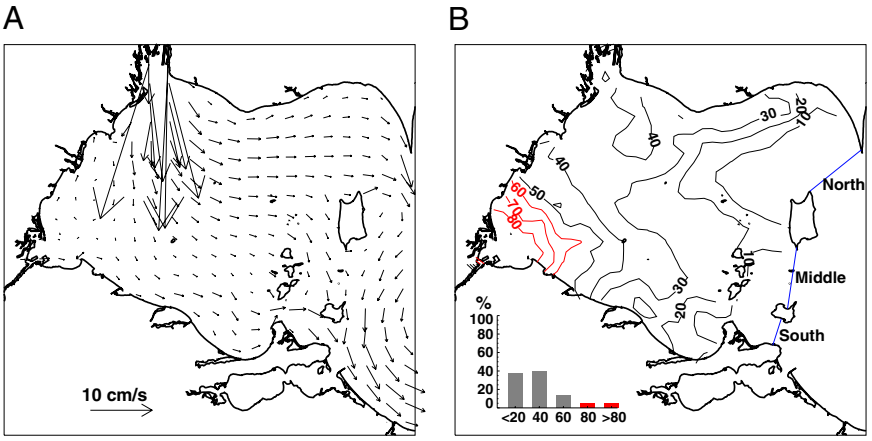

Fig. 3. Depth-averaged circulation (*A*) and residence times (*B*) in days of western basin of Lake Erie in June 2011. Red contours illustrate residence times that exceed the mean hydraulic residence time of the western basin. Histogram shows the percentage of water in the basin with residence times below 20 d, 20–40 d, 40–60 d, 60–80 d, and greater than 80 d.

longer residence times that incubated the bloom, and that warm and quiescent lake conditions after bloom onset allowed *Microcystis* to remain near the top of the water column and prevented flushing of nutrients out of the system. Conversely, data do not support the hypothesis that recent land use and crop choice trends in the watershed contributed to the observed significant increase in the 2011 nutrient loading. In addition, observations show that lake conditions were not unusually warm and quiescent before bloom onset, and the resuspension event immediately preceding the bloom was not of unusual magnitude. Overall, the magnitude of the 2011 bloom was thus caused by a confluence of long-term trends in agricultural nutrient management and extreme meteorological events conducive to bloom formation.

The degree to which the 2011 bloom is a harbinger of future conditions depends on the likelihood of these long-term agricultural trends continuing, and the likelihood of an increased frequency of meteorological conditions such as those observed in 2011.

Lacking policy intervention, many of the socioeconomic forces driving the trends in agriculture and nutrient management practices found to have exacerbated the 2011 bloom are likely to continue, increasing the likelihood of such massive blooms in the future. Factors such as increasing fertilizer costs, however, may provide some economic constraints. Furthermore, although crop choice was not found to have been a contributing factor in 2011, 2012 showed a marked increase in fertilizer-intensive corn acreage in the region (15% increase in Ohio; 4% increase in Michigan) (38). Nationally, planted corn acres were higher than a recent spike in 2007 and the highest since 1937, driven in large part by the high prices for corn resulting from biofuel policy (39). In addition, prospective changes to the CRP would lead to higher land use by agriculture overall (*SI Materials and Methods* and *SI Results and Discussion*). If the 2012 corn acreage is indicative of the future—and policies mandating higher biofuel production and lower CRP acres suggest that it is—then this trend will add to those trends found to have been significant in the 2011 loads.

To determine if precipitation events such as those observed in spring 2011 are more likely to occur in the future, we evaluate spring (March–April–May) daily precipitation over the western Lake Erie basin from 12 Climate Model Intercomparison Project Phase 5 (CMIP5) climate models implementing the Representative Concentration Pathway 8.5 (RCP8.5) scenario (*SI Materials and Methods*, *SI Results and Discussion*, and Table S3) (40). The historical (1986–2005) CMIP5 simulations over the western basin overpredict the current frequency of events >10 mm (Fig. 4) and overestimate the current average springtime precipitation intensity by 30%. Despite this overprediction of the historical period, prior CMIP3 studies have shown that climate model simulations of large scale (>1,000 km) flow patterns can reliably reproduce observations, and multimodel predictions of increased future precipitation intensity are statistically significant (41). Under the future RCP8.5 scenario, the frequency of events of >20 mm, which have an approximately annual recurrence interval based on the observational record, increases by ∼50%, and the frequency of larger storms increases even more, with events >30 mm being twice as frequent. This suggests a potentially even greater increase in the frequency of occurrence of the largest storms, such as the one observed in 2011.

Weak lake circulation and quiescent conditions after bloom onset, as observed in 2011, are also consistent with observed trends of decreasing wind speeds over the continental United States (42) and elsewhere (43), suggesting that the long residence times and quiescent conditions observed in 2011 may not be uncommon in the future. A continuing trend toward lower wind speeds would contribute to the severity of blooms, both

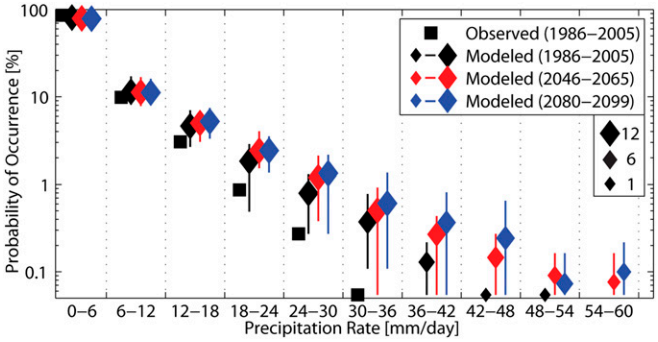

Fig. 4. Probability of daily precipitation intensities for spring (March–April–May) averaged over the western Lake Erie basin (40–43°N, 82–85.5°W) as observed by the Climate Prediction Center (CPC) gridded data (black squares) for the present-day time period (1986–2005), as modeled by a 12-model multimodel average for the same present-day time period (black diamonds) and for two future time periods of 2046–2065 (red diamonds) and 2080–2099 (blue diamonds). Vertical lines represent the range of individual model predictions for those models with a nonzero probability of a given event size. Diamond size represents the number of models included in each calculation (i.e., the number of models with nonzero probabilities for a given event size), ranging from 0 to 12. Individual model members are shown in Fig. S9.

through increasing residence times and decreased mixing in the water column.

In summary, we find that trends in agricultural practices, increased precipitation, weak lake circulation, and quiescent conditions conspired to yield the record-breaking 2011 Lake Erie algal bloom. We further find that all of these factors are consistent with expected future conditions. Lacking the implementation of a scientifically guided management plan designed to mitigate these impacts, we can therefore expect this bloom to indeed be a harbinger of future blooms in Lake Erie.

Materials and Methods

Microcystis biovolume and nutrient concentrations were determined at fixed locations in western Lake Erie, and molecular fingerprints were used to analyze *Microcystis* populations. Data on land use, county-level CRP land area, and crop-level phosphate fertilizer application were obtained from the US Department of Agriculture. Additional county-level nutrient use data were obtained from the Nutrient Use Geographic Information System. Meteorological analysis used data from the University Corporation for Atmospheric Research image archive and the College of DuPage. Daily precipitation observations were obtained from National Oceanic and Atmospheric Administration (NOAA) Climate Prediction Center. Analysis of discharge and phosphorus loading were based on data from the National Center for Water Quality Research at Heidelberg University and flow data from the US Geological Survey. The SWAT model was used to model nutrient loading. Lake Erie wind and temperature data were obtained from the NOAA National Data Buoy Center, and remote sensing lake surface temperature data were obtained from NOAA CoastWatch. Hydrodynamic modeling was conducted using the Beletsky and Schwab model and a particle tracking code was used for residence time calculations and river plume tracking. Present-day and future climate model analyses were based on the CMIP5 data archive. Detailed materials and methods, and references, are available in *SI Materials and Methods*. Information on data availability is provided in *SI Materials and Methods* and *SI Results and Discussion*.

ACKNOWLEDGMENTS. The authors thank Raisa Beletsky, Greg Lang, and David Schwab, who provided modeling support and Todd Marsee for assistance with graphic design. We acknowledge the World Climate Research Programme's Working Group on Coupled Modelling, which is responsible for the Climate Model Intercomparison Project (CMIP), and we thank the climate modeling groups (listed in Table S3 of this paper) for producing and making available their model output. This material is based upon work supported by the National Science Foundation (NSF) under Grants 1039043 and 1313897. Additional support was provided by NSF Grant 0927643 (to D.B.) and the National Oceanic and Atmospheric Administration Center for Sponsored Coastal Ocean Research Grant NA07OAR432000 (to D.B., N.S.B., R.P.R., and D.S.). Support was provided by Lake Erie Protection Fund SG 406-2011 (to J.D.C. and T.B.B.). For CMIP, the US Department of Energy's Program for Climate Model Diagnosis and Intercomparison provided coordinating support and led development of software infrastructure in partnership with the Global Organization for Earth System Science Portals. This paper is Ecofore Lake Erie Contribution Number 12-009 and Great Lakes Environmental Research Laboratory Contribution Number 1646, and Lake Erie Center Contribution Number 2013-09.

1. Smith VH (2003) Eutrophication of freshwater and coastal marine ecosystems: A global problem. *Environ Sci Pollut Res Int* 10(2):126–139.
2. Qin BQ, et al. (2010) A drinking water crisis in Lake Taihu, China: Linkage to climatic variability and lake management. *Environ Manage* 45(1):105–112.
3. Schindler DW, Hecky RE, McCullough GK (2012) The rapid eutrophication of Lake Winnipeg: Greening under global change. *J Great Lakes Res* 38(Suppl 3):6–13.
4. Jöhnk KD, et al. (2008) Summer heatwaves promote blooms of harmful cyanobacteria. *Glob Change Biol* 14(3):495–512.
5. Dolan DM (1993) Point-source loadings of phosphorus to Lake Erie: 1986–1990. *J Great Lakes Res* 19(2):212–223.
6. GLWQA (1978) Great Lakes Water Quality Agreement. Available at http://www.epa.gov/greatlakes/glwqa/1978/index.html. Last accessed March 14, 2013.
7. De Pinto JV, Young TC, McIlroy LM (1986) Great lakes water quality improvement. *Environ Sci Technol* 20(8):752–759.
8. Bertram PE (1993) Total phosphorus and dissolved-oxygen trends in the Central Basin of Lake Erie, 1970–1991. *J Great Lakes Res* 19(2):224–236.
9. DiToro DM, Thomas NA, Herdendorf CE, Winfield RP, Connolly JP (1987) A post audit of a Lake Erie eutrophication model. *J Great Lakes Res* 13(4):801–825.
10. Makarewicz JC (1993) Phytoplankton biomass and species composition in Lake Erie, 1970 to 1987. *J Great Lakes Res* 19(2):258–274.
11. Burns NM, Rockwell DC, Bertram PE, Dolan DM, Ciborowski JJH (2005) Trends in temperature, Secchi depth, and dissolved oxygen depletion rates in the central basin of Lake Erie, 1983–2002. *J Great Lakes Res* 31(Suppl 2):35–49.
12. Rucinski DK, Beletsky D, DePinto JV, Schwab DJ, Scavia D (2010) A simple 1-dimensional, climate based dissolved oxygen model for the central basin of Lake Erie. *J Great Lakes Res* 36(3):465–476.
13. Conroy JD, Culver DA (2005) Do dreissenid mussels affect Lake Erie ecosystem stability processes? *Am Midl Nat* 153(1):20–32.
14. Bridgeman TB, Chaffin JD, Filbrun JE (2013) A novel method for tracking western Lake Erie Microcystis blooms, 2002–2011. *J Great Lakes Res* 39(1):83–89.
15. Bridgeman TB, Penamon WA (2010) Lyngbya wollei in western Lake Erie. *J Great Lakes Res* 36(1):167–171.
16. Strickland T, Fisher L, Korleski C (2010) *Ohio Lake Erie Phosphorus Task Force Final Report* (Ohio Environmental Protection Agency, Columbus, OH).
17. Bierman VJ, Kaur J, DePinto JV, Feist TJ, Dilks DW (2005) Modeling the role of zebra mussels in the proliferation of blue-green algae in Saginaw Bay, Lake Huron. *J Great Lakes Res* 31(1):32–55.
18. Nuisance and Harmful Algae Work Group (2011) *Nuisance and Harmful Algae: 2009–2011 Priority Cycle Report*. (Windsor, Ontario, Canada).
19. Vanderploeg HA, et al. (2001) Zebra mussel (Dreissena polymorpha) selective filtration promoted toxic Microcystis blooms in Saginaw Bay (Lake Huron) and Lake Erie. *Can J Fish Aquat Sci* 58(6):1208–1221.
20. Vanderploeg HA, et al. (2002) Dispersal and emerging ecological impacts of Ponto-Caspian species in the Laurentian Great Lakes. *Can J Fish Aquat Sci* 59(7):1209–1228.
21. Conroy JD, et al. (2005) Temporal trends in Lake Erie plankton biomass: Roles of external phosphorus loading and dreissenid mussels. *J Great Lakes Res* 31(Suppl 2): 89–110.
22. Petrie SA, Knapton RW (1999) Rapid increase and subsequent decline of zebra and quagga mussels in Long Point Bay, Lake Erie: Possible influence of waterfowl predation. *J Great Lakes Res* 25(4):772–782.
23. SOLEC (2012) Dreissenid Mussels: Zebra and Quagga mussels. Available at www.solecregistration.ca/documents/Dreissenid%20Mussels%20DRAFT%20Oct2011.pdf. Accessed March 14, 2013.
24. Smith DA, Matisoff G (2008) Sediment oxygen demand in the central basin of Lake Erie. *J Great Lakes Res* 34(4):731–744.
25. Lu Y, et al. (2010) [delta] 15N values in Lake Erie sediments as indicators of nitrogen biogeochemical dynamics during cultural eutrophication. *Chem Geol* 273(1–2):1–7.
26. Stumpf RP, Wynne TT, Baker DB, Fahnenstiel GL (2012) Interannual variability of cyanobacterial blooms in Lake Erie. *PLoS ONE* 7(8):e42444.
27. Chorus I, Bartram J (1999) *Toxic Cyanobacteria in Water: A Guide to Their Public Health Consequences, Monitoring, and Management* (Taylor & Francis, London).
28. Elser JJ (1999) The pathway to noxious cyanobacteria blooms in lakes: The food web as the final turn. *Freshw Biol* 42(3):537–543.
29. Hendzel LL, Hecky RE, Findlay DL (1994) Recent changes of N-2-fixation in Lake-227 in response to reduction of the N/P loading ratio. *Can J Fish Aquat Sci* 51(10):2247–2253.
30. Tilman D (1982) *Resource Competition and Community Structure* (Princeton Univ Press, Princeton, NJ), pp xi.
31. Smith VH (1983) Low nitrogen to phosphorus ratios favor dominance by blue-green algae in lake phytoplankton. *Science* 221(4611):669–671.
32. Konopka A, Brock TD (1978) Effect of temperature on blue-green algae (cyanobacteria) in lake mendota. *Appl Environ Microbiol* 36(4):572–576.
33. Zohary T, Breen CM (1989) Environmental factors favouring the formation of Microcystis aeruginosa hyperscums in a hypertrophic lake. *Hydrobiologia* 178(3): 179–192.
34. Arnold JG, Srinivasan R, Muttiah RS, Williams J (1998) Large area hydrologic modeling and assessment part I: Model development1. *JAWRA Journal of the American Water Resources Association* 34(1):73–89.
35. Daloğlu I, Cho KH, Scavia D (2012) Evaluating causes of trends in long-term dissolved reactive phosphorus loads to Lake Erie. *Environ Sci Technol* 46(19):10660–10666.
36. Wynne TT, Stumpf RP, Tomlinson MC, Dyble J (2010) Characterizing a cyanobacterial bloom in western Lake Erie using satellite imagery and meteorological data. *Limnol Oceanogr* 55(5):2025–2036.
37. NOAA (2012) Harmful Algal Blooms (HAB) in Lake Erie: Experimental HAB Bulletin Archive. (NOAA, Silver Spring, MD).
38. US Department of Agriculture (2012) Acreage. Available at www.usda.gov/nass/PUBS/TODAYRPT/acrg0612.pdf. Accessed March 14, 2013.
39. US Department of Agriculture (2012) USDA Agricultural Projections to 2021. Available at www.usda.gov/oce/commodity/archive_projections/USDAAgriculturalProjections2021.pdf. Accessed March 14, 2013.
40. Taylor KE, Stouffer RJ, Meehl GA (2012) An overview of Cmip5 and the experiment design. *Bull Am Meteorol Soc* 93(4):485–498.
41. Solomon S Intergovernmental Panel on Climate Change (2007) Climate change 2007: The physical science basis. Contribution of Working Group I to the Fourth Assessment Report of the Intergovernmental Panel on Climate Change (Cambridge Univ Press, Cambridge) pp viii, 996 p.
42. Pryor SC, et al. (2009) Wind speed trends over the contiguous United States, *J Geophys Res-Atmos* 114:D14105.
43. Vautard R, Cattiaux J, Yiou P, Thépaut J-N, Ciais P (2010) Northern hemisphere atmospheric stilling partly attributed to an increase in surface roughness. *Nat Geosci* 3(11):756–761.

Supporting Information

Michalak et al. 10.1073/pnas.1216006110

SI Materials and Methods

In-Lake *Microcystis* Data. *Microcystis* biovolume (milliliters per meter squared) was estimated from six fixed locations in western Lake Erie (1). *Microcystis* colonies were collected in duplicate whole water-column tows at approximate biweekly intervals (April–October) using a 112-μm mesh plankton net in 2002–2011. Biovolume of *Microcystis* in these tows was determined with a settling method and averaged over all sites on a given date. Annual bloom biovolume of *Microcystis* blooms was determined by calculating the area under the curve for plots of biovolume over time, throughout the growing season (1).

Ambient concentrations of nitrogen, phosphorus, and other algal nutrients were determined at six locations at approximately biweekly intervals in 2011. Vertical tube samplers were used to collect integrated water-column samples that were placed on ice and transported to the laboratory within 5 h of collection. Water samples were filtered on 0.45-μm Millipore filters and stored frozen until analysis. Concentrations of dissolved nutrients were determined at the National Center for Water Quality Research in Tiffin, Ohio following standard methods (2) and US Environmental Protection Agency protocols.

Molecular fingerprints were used to analyze similarity of *Microcystis* in the western basin during July–September, with those in the central basin on October 10. DNA collected on 0.45-μm polyvinylidene fluoride filters was extracted using a MoBio Power Water kit (MoBio Laboratories; 14900), and then the 16S–23S rRNA internal transcribed spacer (ITS) gene was PCR amplified following the protocol from ref. 3. The PCR products were visualized on 2% (wt/vol) agarose gel and the *Microcystis* 550-bp band (3) was excised, PCR amplified again, and visualized on a 2% (wt/vol) agarose gel to ensure purity. Molecular fingerprints were generated using denaturing gradient gel electrophoresis with a 30–40% denaturing gradient (3).

Microcystin concentration was determined using ELISA (Abraxis; 520011) following cell lysis (Abraxis; Quik-lyse kit 529911QL) of unfiltered water-column samples, as in ref. 4. This microcystin analysis is congener independent, therefore representing the total microcytin concentration.

Land Use Data. Annual county-level data for corn, winter wheat, and soybean acres planted are available from US Department of Agriculture (USDA)'s National Agricultural Statistics Service (NASS) using the Quick Stats tool available at https://explore.data.gov/Agriculture/Quick-Stats/ddcm-63jr. To generate acreage estimates for the western Lake Erie watershed, county totals were summed across all counties that overlap the watershed.

Data on county-level Conservation Reserve Program (CRP) land area are available online as Excel spreadsheet files from the Farm Service Agency CRP statistics webpage (available at www.fsa.usda.gov). County totals were summed across all counties that overlap the western Lake Erie watershed.

Fertilizer Use Data. Throughout the manuscript, "phosphate" refers to fertilizer applications and "phosphorus" refers to any form of phosphorus in water, including orthophosphate and dissolved organic phosphorus.

Data on crop-level phosphate fertilizer applications for 1997–2010 are from USDA's Agricultural Resource Management Survey (ARMS). The data were compiled from https://explore.data.gov/Agriculture/Quick-Stats/ddcm-63jr. The data represent state-level averages from sampled farms. Phosphate data from ARMS are not available for the major crops in the watershed for 2011; the most recent data are from 2010. Phosphate fertilizer data are reported as amounts of P_2O_5.

A second source of data on fertilizer use for 2007–2010 is from the International Plant Nutrition Institute. These data were developed for the Nutrient Use Geographic Information System (NuGIS) and represent estimates of farm-level nutrient applications for counties in the western Lake Erie watershed. Whereas the recent data are not publicly available, county-level estimates at 5-y intervals from 1987 to 2007 are available to the public. County totals were summed across all counties that overlap the western Lake Erie watershed to obtain watershed-level estimates.

Precipitation Data. Meteorological analysis for spring 2011 is based on a combination of satellite, radar, and surface analysis from the University Corporation for Atmospheric Research image archive (www.mmm.ucar.edu/imagearchive/) and the College of DuPage (http://weather.cod.edu/).

Daily precipitation observations for 1986–2005 (Fig. 4) are based on the National Oceanic and Atmospheric Administration (NOAA) Climate Prediction Center (CPC) daily US Unified precipitation dataset. The CPC daily Unified precipitation is a 0.25° × 0.25° gridded product available from 1948 to 2006 derived from three sources, including National Climatic Data Center (NCDC) station data, the CPC dataset, and daily accumulations of hourly precipitation (data available at www.esrl.noaa.gov/psd/data/gridded/data.unified.html). Present-day observations were spatially averaged over the western Lake Erie basin to represent the watersheds of interest (40–43°N, 85.5–83°W). Observational averages (Fig. 4 and Fig. S9) reflect an average from 1986 to 2005, the defined Climate Model Intercomparison Project Phase 5 (CMIP5) present-day analysis time period. Whereas 2011 is not in the Unified CPC dataset, real-time data are available for 2011 and implemented for the May 2011 event analysis as described in the previous paragraph.

Nutrient Loading Data. Analysis of long-term trends and 2011 discharge and phosphorus loading were performed using the Maumee River dataset of the National Center for Water Quality Research at Heidelberg University (NCWQR) and flow data from the US Geological Survey, both from a site at Waterville, Ohio (USGS 04193500). The NCWQR dataset contains near-daily observations of sediment, nutrients, and major ions with two to four observations per day during periods of storm runoff, and contains more than 16,000 samples between 1975 and 2011. Parameters include total phosphorus (TP) and dissolved reactive phosphorus (DRP). Based on results from special studies on a smaller number of samples, particulate phosphorus (PP) was estimated as $PP = TP - 1.1 \times DRP$. Phosphorus loads are reported as metric tons of P.

The Maumee data were converted to a complete daily time series by discharge-weighted averaging of concentrations for days with multiple samples. Daily discharge for 2011 is shown in Fig. S4. Gaps in phosphorus data were filled using linear interpolation if the gap was less than 6 d long or by regression models relating concentration to flow, long-term trend, and seasonality if longer than 6 d long. The daily series were collapsed to monthly series, which are used for trend analysis.

Long-term trends (1995–2011) and net changes were determined by regression of monthly load and discharge-weighted mean concentration (load/discharge) against decimal time. Results were verified using more complex regression models involving ln

(concentration) as a function of ln(discharge), time, and seasonality represented by sine and cosine terms in $2\pi t$ and $4\pi t$, where t is decimal time (5, 6). Table S2 shows the results of this regression analysis.

Analysis of 2011 loading was performed using a FORTRAN program that steps through the daily time series, computing the total discharge and loads for a specified length of time (111 or 15 d for this study). The results were then sorted from high to low and the corresponding percentile in the overall distribution was computed for the period that ended June 8, 2011, the last day of the period of storm runoff.

Soil and Water Assessment Tool Model. The Soil and Water Assessment Tool (SWAT), developed by the USDA, is a process-based watershed model with spatially explicit parameterization (7, 8). SWAT models forecast hourly, daily, monthly, or annual flow, discharge, sediment, and nutrient loads for each subwatershed (often around 10,000 ha) and for an entire watershed. It is a continuous time and long-term model to predict the impact of agricultural management on flow, discharge, sediment, nutrient, and chemical yields (7). SWAT is driven with weather data (i.e., precipitation and air temperature), and approximates the hydrologic cycle (i.e., surface runoff, infiltration, and evapotranspiration), plant growth, water quality constituents (i.e., nitrogen, phosphorus, pesticides, and bacteria), and agricultural management schemes (i.e., fertilizer/manure application and tillage practices).

Lake Erie Temperature and Wind Data. Wind and temperature data from a buoy located in the central basin of Lake Erie were analyzed to assess in-lake meteorological conditions during the spring and summer in 2011. Hourly data on wind speed and water temperature were downloaded from the NOAA National Data Buoy Center (NDBC) website (www.ndbc.noaa.gov/station_page.php?station=45005) for Station 45005 (41.677 N 82.398 W), a 3-m discus buoy operated in the middle of the central basin of Lake Erie. The data are available for the years 2002–2011.

Wind stress in units of Pascals (τ) is determined from wind speed based on the approach in ref. 9:

$$\tau = \rho \times w^2 \times [0.001 \times (0.69 + 0.081 \times w)],$$

where ρ is the air density, estimated as 1.25 kg·m^{-3}, w is the mean hourly wind speed in m/s, and the term in square brackets is an empirical drag coefficient. Wind stress and water temperature were daily averaged (i.e., over 24 h).

Days with average wind stress less than 0.05 Pa and average water temperature greater than 15 °C were classified as promoting growth, whereas periods with average wind stress greater than 0.1 Pa and/or average water temperature less than 15 °C were classified as limiting growth (9).

Additionally, three specific time periods were identified for years where the bloom initiation date was known (2002, 2003, 2008, and 2011): prebloom, bloom onset, and postonset. The approximate dates of bloom initiation, determined based on dates reported in the literature (9–12), were August 28, 2002; August 12, 2003; August 14, 2008; and July 15, 2011, respectively.

The prebloom period was defined as the time from the first occurrence of the growth-promoting conditions until two weeks before bloom initiation. The bloom onset period was defined as a four-week window around the date of bloom initiation. The postonset period is defined as starting two weeks after bloom initiation and lasting until the last occurrence of growth-promoting conditions. The percent of time with growth-promoting and growth-limiting conditions was calculated for each of these three periods for the four years with known bloom initiation dates.

Statistical significance was assessed using a difference in sample proportions test, comparing 2011 conditions to pooled statistics from 2002, 2003, and 2008, examining the proportion of days in each period where conditions were either growth promoting or growth limiting, depending on the analysis. No significant temporal autocorrelation was found in the observations, confirming the validity of this test.

Remotely sensed lake surface temperature data from the NOAA CoastWatch were also examined for all of Lake Erie for 1992–2011 and for the western basin specifically for the years 2009–2011 (data available from http://coastwatch.glerl.noaa.gov/; Fig. S5).

Lake Hydrodynamic Model. The 3D hydrodynamic circulation model developed by Beletsky and Schwab (13) was used to represent circulation in Lake Erie. The model is based on the Princeton Ocean Model (14) and is a nonlinear, hydrostatic, fully 3D, primitive equation, finite difference model. The model uses time-dependent wind stress and heat flux forcing at the surface, free-slip lateral boundary conditions, and quadratic bottom friction. The drag coefficient in the bottom friction formulation is spatially variable and is calculated based on the assumption of a logarithmic bottom boundary layer using depth-dependent bottom roughness that varies from 0.1 cm in deep water to 1 cm in shallow water. Horizontal diffusion is calculated with a Smagorinsky eddy parameterization with a multiplier of 0.1 to give a greater mixing coefficient near strong horizontal gradients. The Princeton Ocean Model employs a terrain following vertical coordinate system (sigma-coordinate). The equations are written in flux form, and the finite differencing is done on an Arakawa-C grid using a control volume formalism. The finite differencing scheme is second order and centered in space and time (leap-frog). The model includes ref. 15's level 2.5 turbulence closure parameterization.

The hydrodynamic model of Lake Erie has 21 vertical levels (with equal spacing from surface to bottom) and a uniform horizontal grid size of 2 km (Fig. S6). The model was driven by observed winds and tributary flows. Daily inflows from 22 tributaries and outflows at the Niagara River and Welland Canal were incorporated as boundary conditions (16). The model also incorporates an empirical ice model (16), which reduces momentum flux: wind stress is reduced by 0.5 times the ice concentration. The model was validated with observations of water level and lake surface temperature.

Lake Particle Transport Model. The 3D particle trajectory code is based on the second order accurate horizontal trajectory code described by ref. 17, with the addition of vertical position tracking. It uses currents from the 3D circulation model of Lake Erie. Particles in the model are neutrally buoyant and follow the local currents. Particles are reflected back into the interior after collisions with model boundaries. Horizontal and vertical diffusion was introduced via Smagorinsky (with coefficient of 0.005) and random-walk approaches, respectively. Vertical diffusion was set at 5×10^{-4} m^2/s.

Lake Residence Times and River Plume Tracking. Particles were released at lake surface for two cases: (*i*) monthly basin-wide instantaneous releases and (*ii*) Maumee River and Detroit River mouth continuous 30-d release for June 2011.

In case *i*, residence times were investigated as a function of location and month (Fig. S7). In each month, particles were distributed across the western basin (20 particles per grid element) on the first day of each month, and trajectories were computed for each particle until it left the western basin.

In case *ii*, particles were released hourly from the Maumee and Detroit River mouths for the period June 1 to July 1, 2011 (20 particles per hour for 30 d; Fig. S8). Water originating from the Maumee and Detroit Rivers was tracked separately to elucidate mixing between the two sources and to determine the pathway by which their respective waters leave the basin.

Climate Model Output. Present-day and future climate model analysis was based on the Coupled Model Intercomparison Project Phase 5 (CMIP5) model data archive (18) (data available at http://cmip-pcmdi.llnl.gov/index.html). All model output was spatially averaged over the western Lake Erie basin. A total of 20 models in the CMIP5 archive have daily precipitation rates available, and one ensemble member (r1i1p1) for each model was selected for this analysis. Of these 20 models with daily precipitation rates, only 12 models had available future simulations using the Representative Concentration Pathway (RCP8.5) emissions scenario. The RCP8.5 emissions scenario projects greenhouse gas emissions with a continuous rise in radiative forcing to about 8.5 Watts per square meter in 2100 (19) and therefore represents an aggressive warming scenario. The 12 models selected for this analysis are detailed in Table S3.

SI Results and Discussion

May 25–27 Precipitation Event. The precipitation during May 25–27, 2011 over the Maumee and Sandusky river basins was produced by convective cloud clusters embedded in a synoptic scale low-pressure system. The center of circulation originated over the southern Great Plains on May 25, 2011, and propagated to the north and east over the following 2 d. Convection was concentrated along a lower-tropospheric stationary front that stretched from the low-pressure center to the northeast over the Maumee River watershed (Fig. S3). By 1200 coordinated universal time (UTC) on the 25th, a cluster of convective cells had formed along this boundary and subsequently moved to the north and east, reaching the Maumee basin by 1730 UTC (Fig. S3*A*). Over the following 10 h, convection continued to develop west and south of Lake Erie, moving in near continuous fashion over the Maumee and Sandusky river basins (Fig. S3*B*). During this time, a south–north oriented line of intense convective precipitation developed over Illinois associated with very strong south-to-north low level water vapor transport along and ahead of the surface cold front. Precipitation from this convective line reached the western shore of Lake Erie at ~0600 UTC on May 26 (Fig. S3*C*) and rapidly moved to the northeast, exiting the region by ~0800 UTC. Between 0800 UTC on May 26 and 0400 UTC on May 27, the center of circulation passed south of Lake Erie and produced a final set of relatively unorganized convective precipitation cells between 1600 UTC on May 26 and 0300 UTC on May 27 (Fig. S3*D*).

Land Use. Three main agricultural crops are grown in the western Lake Erie watershed: soybeans, corn, and winter wheat (Fig. S2). Substantial cropland also resides in the Conservation Reserve Program (CRP) under contracts that expire in different years (Fig. S2). The national trends in land use, since 2007, show an increase in corn and a decrease in CRP. Specifically, corn cropland grew by over 3.655 million hectares (11%) when comparing average annual area before (1997–2006) and after (2008–2011) the anomalous spike in corn cropland in 2007. CRP land area declined by 2.9 million hectares (20%) since 2007.

Trends in the western Lake Erie watershed, however, deviate sharply from the national trends. Based on county-level data for the watershed from the National Agricultural Statistics Service, average corn area for 2008–2011 decreased slightly relative to 1997–2006, from 959,000–957,000 ha per year. A minor upward trend occurred annually after 2007, with hectares increasing from 944,000 in 2008 to 967,000 in 2011 (2% increase). The watershed did experience the 2007 spike, with 1,114,000 ha planted in corn. A slight downward trend in CRP area occurred in the watershed, with hectares declining from 128,812 in 2007 to 114,806 in 2011 (11% decrease). Fig. S2 illustrates these trends.

Fertilizer Use. Two perspectives are relevant on phosphate fertilizer use: a comparison across the three main crops grown in the watershed and evidence on recent applications. The data on crop-level phosphate applications for 1997–2010 are from USDA's ARMS. We used state-level data from Ohio farms (the majority of the watershed is in Ohio) because county-level data are not available. ARMS does not collect data on every crop each year. Average phosphate applications are as follows: corn receives 78.7 $kg{\cdot}ha^{-1}{\cdot}y^{-1}$ (as P_2O_5) based on 9 y of data; soybeans receive 58.1 $kg{\cdot}ha^{-1}{\cdot}y^{-1}$ based on 8 y of data; and wheat receives 72.2 $kg{\cdot}ha^{-1}{\cdot}y^{-1}$ based on 7 y of data. Intensification of corn production—for example, (*i*) extending to 2 y of corn before growing soybeans in a corn–soybean rotation, (*ii*) moving from a corn–soybean rotation to continuous corn, or (*iii*) converting CRP land to corn production—would result in higher phosphate applications on farm fields.

Phosphate application data for the three crops are not available from ARMS for 2011 (only barley and sorghum are available for 2011); the most recent data are for 2010. In Ohio and Michigan, annual phosphate applications on corn fields were markedly lower in 2010 than during 1997–2005. The Ohio rate was 71.7 $kg{\cdot}ha^{-1}{\cdot}y^{-1}$ versus the 1997–2005 average of 79.6 $kg{\cdot}ha^{-1}{\cdot}y^{-1}$, whereas the Michigan rate was 35.9 $kg{\cdot}ha^{-1}{\cdot}y^{-1}$ versus the 1997–2005 average of 52.5 $kg{\cdot}ha^{-1}{\cdot}y^{-1}$. At the same time, other estimates of phosphate fertilizer applications in 2010 from the International Plant Nutrition Institute were higher than in the three previous years, 2007–2009. An estimated 83,814 tons were applied, in total, to farmland in the western Lake Erie watershed in 2010. The second highest level was 79,246 tons in 2007.

Dominance of Maumee River Nutrient Loading. The nutrient loading analysis was focused on the Maumee River because it dominates nonpoint source loading to the western basin of Lake Erie, where the *Microcystis* algal blooms originate.

The Maumee River contributes about 5% of discharge, but nearly 50% of phosphorus loading to the western basin. The other major loading source to the western basin is the Detroit River, which also contributes almost 50% of the phosphorus load, but more than 90% of the discharge. Because of the difference in discharge, the phosphorus concentrations in the Detroit River plume are much lower than those in the Maumee River plume. This means that the Detroit River concentrations are too low to make a significant contribution to major cyanobacteria blooms in the western basin of Lake Erie. Based on annual loads measured by the NCWQR between 2002 and 2011, the Sandusky River, which enters Lake Erie at the western end of the central basin, had 24% of both the TP and the DRP load of the Maumee River, and the Raisin River, adjacent to the Maumee to the north, had only 5% of the TP load and 6% of the DRP load of the Maumee. During the first half of 2011, the Sandusky River discharge was 30% of the Maumee River discharge, the TP load was 29% of the Maumee River load, and the DRP load was 27%. Cumulative loads of DRP for Maumee and Sandusky during the first half of 2011 are shown in Fig. S4.

Phosphorus loading from the Sandusky River may have helped support the late development of the 2011 bloom in the central basin. However, the Sandusky River discharges to the relatively large Sandusky Bay, where significant processing of phosphorus occurs before the water enters the central basin proper. Sandusky Bay often has its own algal blooms, but these are typically *Planktothrix*, a different alga. The fact that this alga was not detected in the central basin bloom indicates that the influence of the Sandusky River on the 2011 bloom was secondary at best, through phosphorus recycling in the lake.

SWAT Modeling. We model the Maumee watershed to investigate the effect of storm events and agricultural management practices on nutrient delivery to Lake Erie. SWAT was previously calibrated and confirmed for the Maumee watershed for discharge, sediment, and total and dissolved reactive phosphorus from 1998 to 2001 (20). Building on ref. 20, we extended the simulation period

(1970–2011) with calibration (1991–2011) and validation (1975–1990) to further explore the impact of weather and management scenarios on phosphorus loads. Temporal variation of agricultural practices, crop choices, and fertilizer application rates (21, 22) were represented for the 40-y simulation. We use meteorological information from 2011 and agricultural management input to investigate their contributions on nutrient delivery in the 2011 event. Precipitation data were taken from a single representative NOAA station in Fort Wayne, Indiana (Station ID:US1INAL0039) to drive the model scenarios. To enhance or reduce precipitation intensities, we multiplied observed intensities in April and May 2011 by 1.2 or 0.8, respectively. For the agricultural management practices, we assumed that all farmers in the watershed apply fertilizer on either April 15, May 5, or May 21 and select either no till or conventional tillage. Tillage practices in SWAT are represented by modifying the curve number (CN2) and overland roughness (23). The 1970–2011 model simulation includes the parameter changes described above during the whole simulation period.

Lake Erie Temperature and Wind Data. The analysis of bloom-promoting and bloom-limiting conditions shows that 2011 was less warm and quiescent (i.e., less bloom promoting) during the pre-bloom period than other years (51% relative to 64–71% in other years, $p = 0.017$). For the bloom onset period, 2011 was unremarkable with respect to strong wind conditions; it was under bloom-limiting conditions (i.e., high wind stress and/or temperature) 3.5% of the time, compared with 3.3–10.3% in other years ($p = 0.32$).

As an analysis of robustness, different start dates for the pre-bloom period were also tested: from the first time under growth-limiting conditions after April 1, from the mean date of first growth-limiting conditions (May 4), and from 2 and 3 mo before the bloom onset period. The results above are consistent across these pre-bloom period start dates.

Lake-wide summer lake surface temperatures in 2011 were about 3 °C above 1992–2011 climatological average (Fig. S5). In the western basin specifically, the 2011 summer peak temperature values reached 27 °C and exceeded that of 2010 by 1.2 °C for about 2 wk.

Future Land Use. Incentives and opportunities to expand corn production are expected to increase over the next 5 to 10 y. Under the Energy Independence and Security Act of 2007, the Renewable Fuel Standard program requires blending a certain amount of biofuel with gasoline (data available from www.epa.gov/oms/fuels/renewablefuels/index.htm). Under the standard, the eligible amount of corn ethanol rises steadily from 9 billion gallons in 2008 to 15 billion gallons in 2015, and it remains there through 2022. (A future rulemaking by the US Environmental Protection Agency will specify conditions after 2022.) Consequently, corn cropland in the United States likely will continue to increase through 2015 and then will (roughly) plateau.

Features of the CRP will tend to support an expansion of crop production in the western Lake Erie watershed. The CRP is a voluntary program in which individual landowners enroll agricultural land in the reserve rather than farming the land. CRP contracts range from 10 to 15 y, and landowners receive payments for their enrolled acreage. CRP contracts continue to expire in the watershed, with 78% of current CRP land (almost 90,000 ha) eligible to return to crop production between 2012 and 2018. Data on contract expirations are available online as Excel spreadsheet files from the Farm Service Agency CRP statistics webpage (available at www.fsa.usda.gov). More generally, the US Congress is considering a new farm bill that would apply through 2017. The leading bills in both houses would shrink the maximum area in the CRP by more than 20%, from 12.9 million hectares in 2012 to 10.1 million hectares in 2017 (for the Senate bill, see http://hdl.loc.gov/loc.uscongress/legislation.112s3240; and for the House bill, see http://hdl.loc.gov/loc.uscongress/legislation.112hr6083. Shrinkage of the program would imply that, through at least 2017, land area in new CRP contracts would not replace the land in expiring contracts. CRP thus will serve as a "new" source of cropland in support of the biofuel boom.

With corn's requirement for phosphate fertilizer, a credible projection for the next decade is that the agricultural land base will create greater potential for phosphorus loadings in western Lake Erie. The relationship between land use and the near-future scenarios of climate change (2046–2065) is less clear and may depend on changes in biofuel production technology. Whether corn continues as a vital feedstock and the environmental consequences of alternative feedstocks are difficult to forecast accurately for that time period.

Climate Model Output. For future climate scenarios, we define two time periods: the near future (2046–2065) and the end of century (2080–2099). Individual CMIP model daily precipitation rates are shown for the historical and two future time horizons (Fig. S9). Nearly all models (except for the Norwegian Climate Center Earth System Model) overpredict the intensity of precipitation with rates above 10 $mm \cdot d^{-1}$. The models estimate that intensity will increase in the both the near-future and end-of-century simulations.

1. Bridgeman TB, Chaffin JD, Filbrun JE (2013) A novel method for tracking western Lake Erie Microcystis blooms, 2002–2011. *J Great Lakes Res* 39(1):83–89.
2. Eaton AD, Franson MAH (2005) *Standard Methods for the Examination of Water and Wastewater* (Amer Public Health Assn, Washington, DC).
3. Janse I, Meima M, Kardinaal WEA, Zwart G (2003) High-resolution differentiation of Cyanobacteria by using rRNA-internal transcribed spacer denaturing gradient gel electrophoresis. *Appl Environ Microbiol* 69(11):6634–6643.
4. Poste AE, Hecky RE, Guildford SJ (2011) Evaluating microcystin exposure risk through fish consumption. *Environ Sci Technol* 45(13):5806–5811.
5. Cohn TA (2005) Estimating contaminant loads in rivers: An application of adjusted maximum likelihood to type 1 censored data. *Water Resour Res* 41(7):W07003.
6. Schwarz GE, Hoos AB, Alexander RB, Smith RA (2006) The SPARROW Surface Water-Quality Model: Theory, Applications and User Documentation. In *US Geological Survey, Techniques and Methods* (US Geological Survey, Reston, VA). Available at http://pubs.usgs.gov/tm/2006/tm6b3. Last accessed March 14, 2013.
7. Gassman PW, Reyes MR, Green CH, Arnold JG (2007) The soil and water assessment tool: Historical development, applications, and future research directions. *T Asabe* 50(4):1211–1250.
8. Tripathi MP, Panda RK, Raghuwanshi NS, Singh R (2004) Hydrological modelling of a small watershed using generated rainfall in the soil and water assessment tool model. *Hydrol Processes* 18(10):1811–1821.
9. Wynne TT, Stumpf RP, Tomlinson MC, Dyble J (2010) Characterizing a cyanobacterial bloom in western Lake Erie using satellite imagery and meteorological data. *Limnol Oceanogr* 55(5):2025–2036.
10. Millie DF, et al. (2009) Late-summer phytoplankton in western Lake Erie (Laurentian Great Lakes): Bloom distributions, toxicity, and environmental influences. *Aquat Ecol* 43(4):915–934.
11. Rinta-Kanto JM, et al. (2005) Quantification of toxic Microcystis spp. during the 2003 and 2004 blooms in western Lake Erie using quantitative real-time PCR. *Environ Sci Technol* 39(11):4198–4205.
12. Vincent RK, et al. (2004) Phycocyanin detection from LANDSAT TM data for mapping cyanobacterial blooms in Lake Erie. *Remote Sens Environ* 89(3):381–392.
13. Beletsky D, Schwab DJ (2001) Modeling circulation and thermal structure in Lake Michigan: Annual cycle and interannual variability. *J Geophys Res-Oceans* 106(C9):19745–19771.
14. Blumberg AF, Mellor GL (1987) A description of a three-dimensional coastal ocean circulation model. In *Three-Dimensional Coastal Ocean Models, Coastal Estuarine Sci.*, ed Heaps NS (American Geophysical Union, Washington, DC), pp. 1–16.
15. Mellor GL, Yamada T (1982) Development of a turbulence closure-model for geophysical fluid problems. *Rev Geophys* 20(4):851–875.
16. Schwab DJ, Beletsky D, DePinto J, Dolan DM (2009) A hydrodynamic approach to modeling phosphorus distribution in Lake Erie. *J Great Lakes Res* 35(1):50–60.
17. Bennett JR, Clites AH (1987) Accuracy of trajectory calculation in a finite-difference circulation model. *J Comput Phys* 68(2):272–282.
18. Taylor KE, Stouffer RJ, Meehl GA (2012) An overview of Cmip5 and the experiment design. *Bull Am Meteorol Soc* 93(4):485–498.
19. Moss RH, et al. (2010) The next generation of scenarios for climate change research and assessment. *Nature* 463(7282):747–756.

20. Bosch NS, Allan JD, Dolan DM, Han H, Richards RP (2011) Application of the Soil and Water Assessment Tool for six watersheds of Lake Erie: Model parameterization and calibration. *J Great Lakes Res* 37(2):263–271.
21. Han H, Allan JD, Bosch NS (2012) Historical pattern of phosphorus loading to Lake Erie watersheds. *J Great Lakes Res* 38(2):289–298.
22. Ruddy BCL, Lorenz DL, Mueller DK (2006) County-level estimates of nutrient inputs to the land surface of the conterminous United States, 1982–2001 (US Geological Survey, Reston, VA).
23. Arabi M, Frankenberger JR, Enge BA, Arnold JG (2008) Representation of agricultural conservation practices with SWAT. *Hydrol Processes* 22(16):3042–3055.

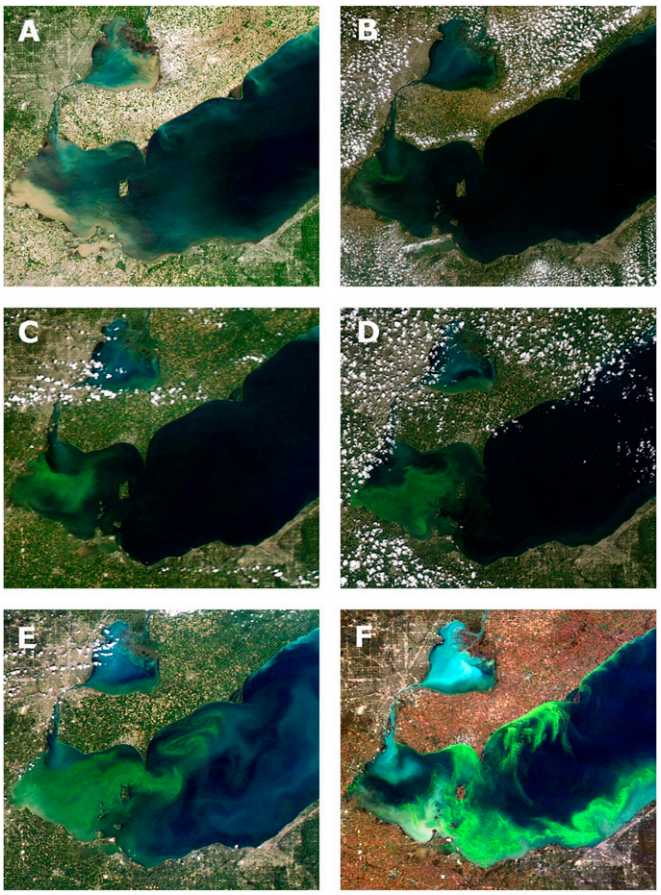

Fig. S1. Progression of Moderate Resolution Imaging Spectroradiometer (MODIS) satellite images of the western basin of Lake Erie. (*A*) June 1, 2011. This image was taken after the peak of the late May high flow event in the Maumee River and shows the plume of suspended solids and associated nutrients from the river associated with that event. (*B*) July 19, 2011. This image was taken at the beginning of the *Microcystis* bloom. It shows that the bloom started along the western shore of the western basin, shortly after a moderate wind-driven bottom sediment resuspension event along the western shore. (*C*) July 31, 2011, approximately 2 wk after the bloom was first initiated. This image shows how the bloom has spread through much of the southern western basin. It also shows how the large flow from the Detroit River is keeping the bloom from spreading to the north. The Detroit River plume is also seen to be short circuiting to the central basin through the north passage between Point Pelee and Pelee Island. (*D*) August 11, 2011. This image shows the bloom spreading east toward the central basin. It also shows a smaller separate bloom from Lake St. Clair beginning to be transported through the Detroit River to the western basin. (*E*) September 3, 2011. This image shows the bloom expanding into the central basin and a second phase of the bloom forming along the northern shore of the central basin. (*F*) October 9, 2011. This image shows the decline of the bloom in the western basin, as it is diluted by the Detroit River plume transporting a whiting event from Lake St. Clair (precipitation of CaCO3 as pH and temperature increase) into the western basin. The bloom is still evident along both the north and south shorelines of the central basin. [Images courtesy of University of Wisconsin-Madison Space Science and Engineering Center.]

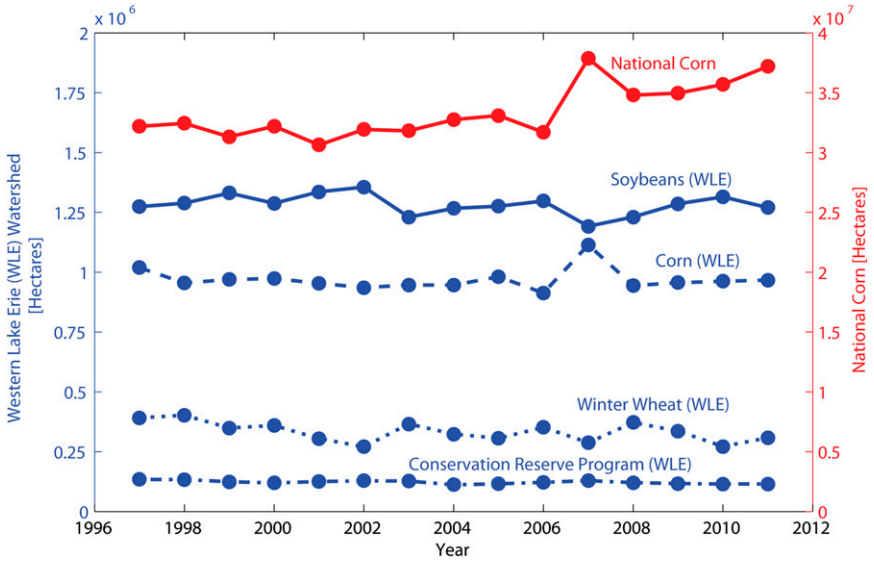

Fig. S2. Major agricultural land uses in western Lake Erie watershed and national corn cropland, 1997–2011.

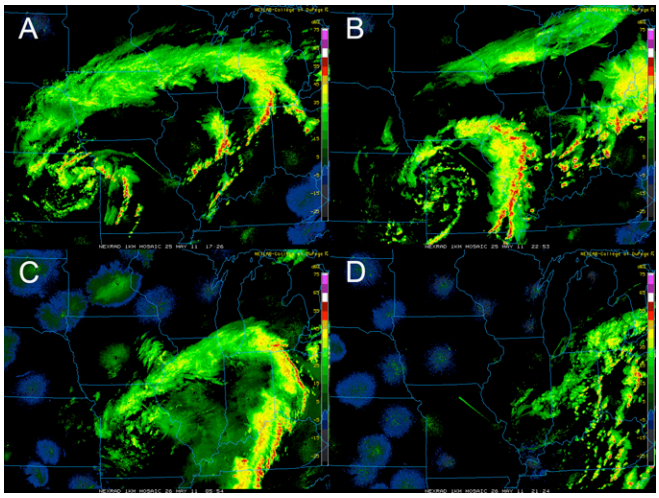

Fig. S3. Radar composite on (*A*) May 25, 2011 at 1730 UTC, (*B*) May 25, 2011 at 2300 UTC, (*C*) May 26, 2011 at 0600 UTC, and (*D*) May 26, 2011 at 2130 UTC.

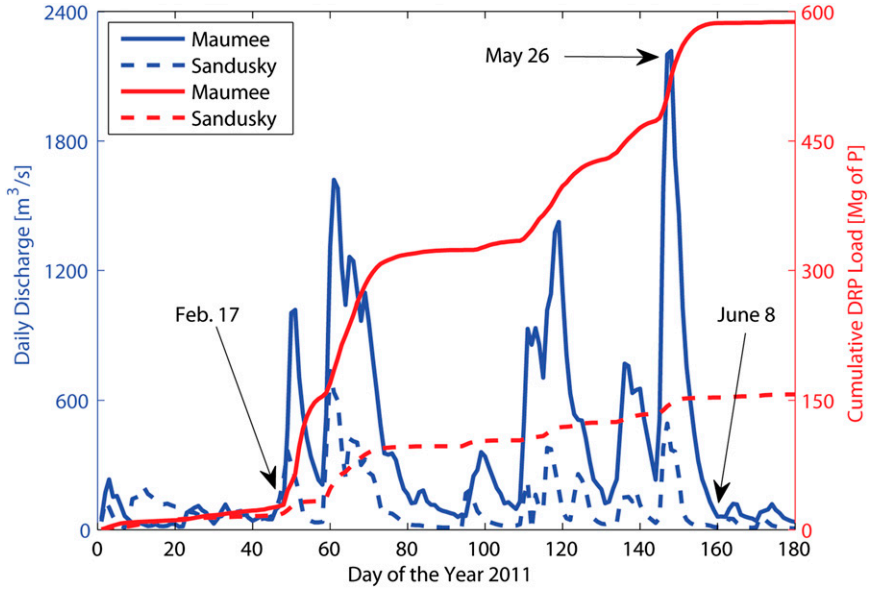

Fig. S4. Maumee River and Sandusky River daily discharge and cumulative DRP loading (as tons of P) for the first half of 2011. Extremely high flows occurring in February through June led to massive DRP loading. The Maumee loading to the western basin is approximately four times larger than the loading from the Sandusky to the central basin.

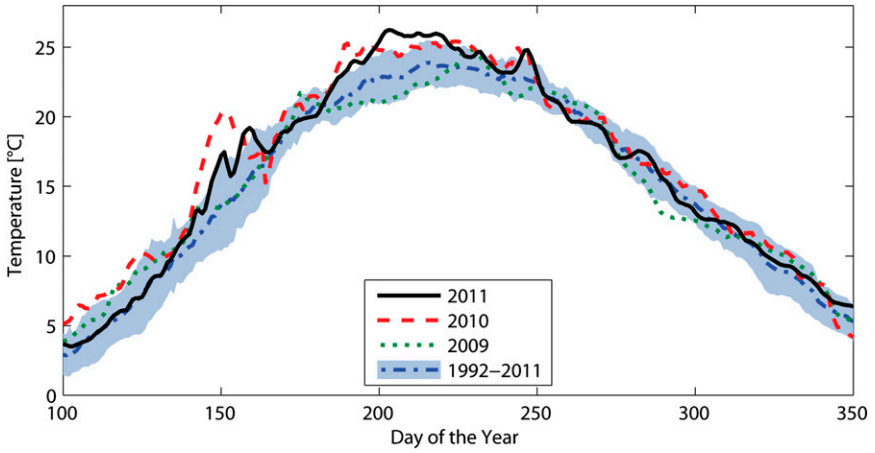

Fig. S5. Lake-average surface water temperature in 2009, 2010, and 2011 relative to the 1992–2011 climatology. Shaded area represents ±1 SD of the 1992–2011 observations.

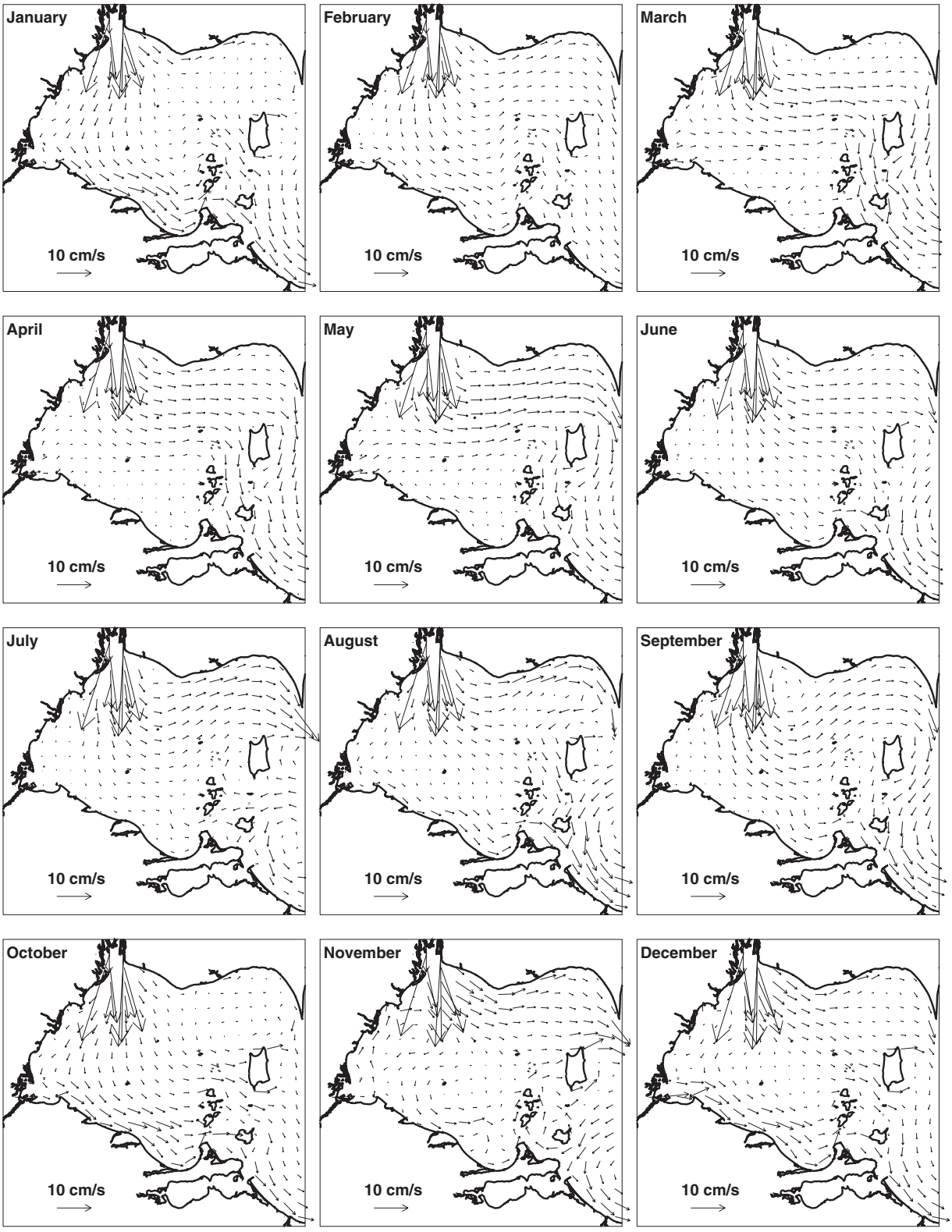

Fig. S6. 2011 monthly mean circulation (depth averaged) in the western basin of Lake Erie.

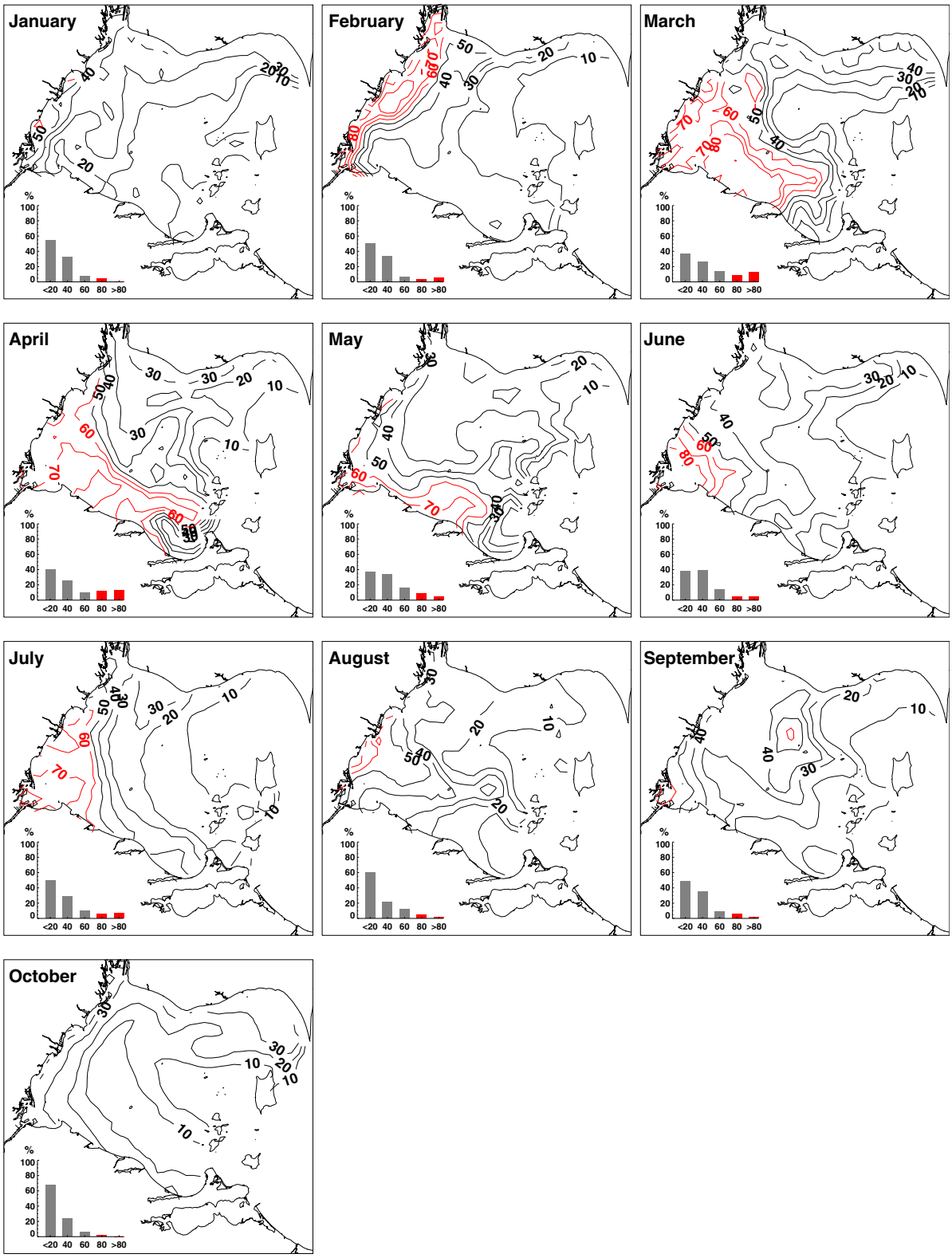

Fig. S7. 2011 residence times of western basin Lake Erie water (in days) for each month. Red contours indicate residence times that exceed the estimated mean hydraulic residence time for the basin (53 d for January–October period). Histograms in the lower left corner of each plot show the percentage of water in the basin with residence times below 20 d, 20–40 d, 40–60 d, 60–80 d, and greater than 80 d.

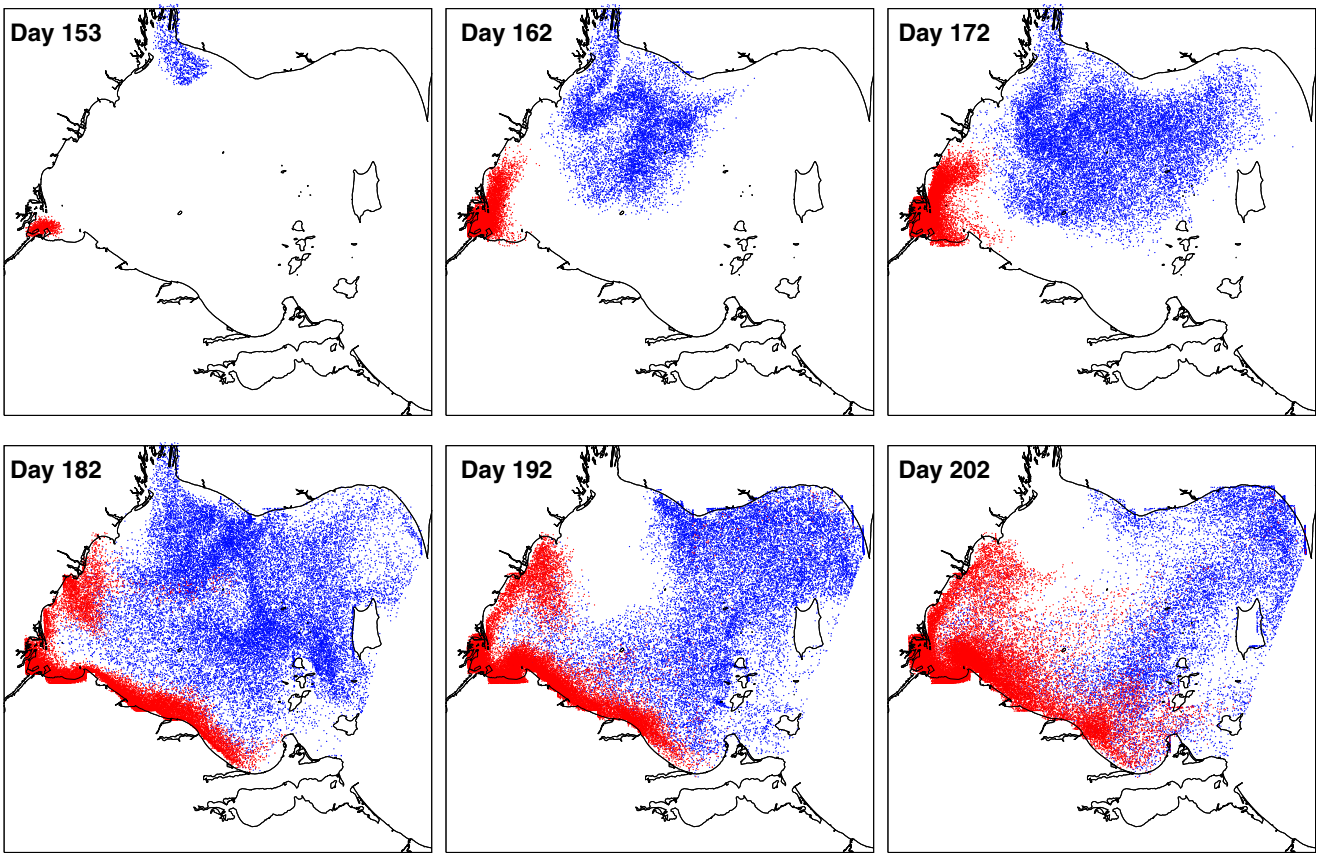

Fig. S8. Particle release tracking the Maumee River (red) and Detroit (blue) River water. Particles are released hourly from each river mouth for a 30-d period starting on June 1, 2011 (Julian Day 152).

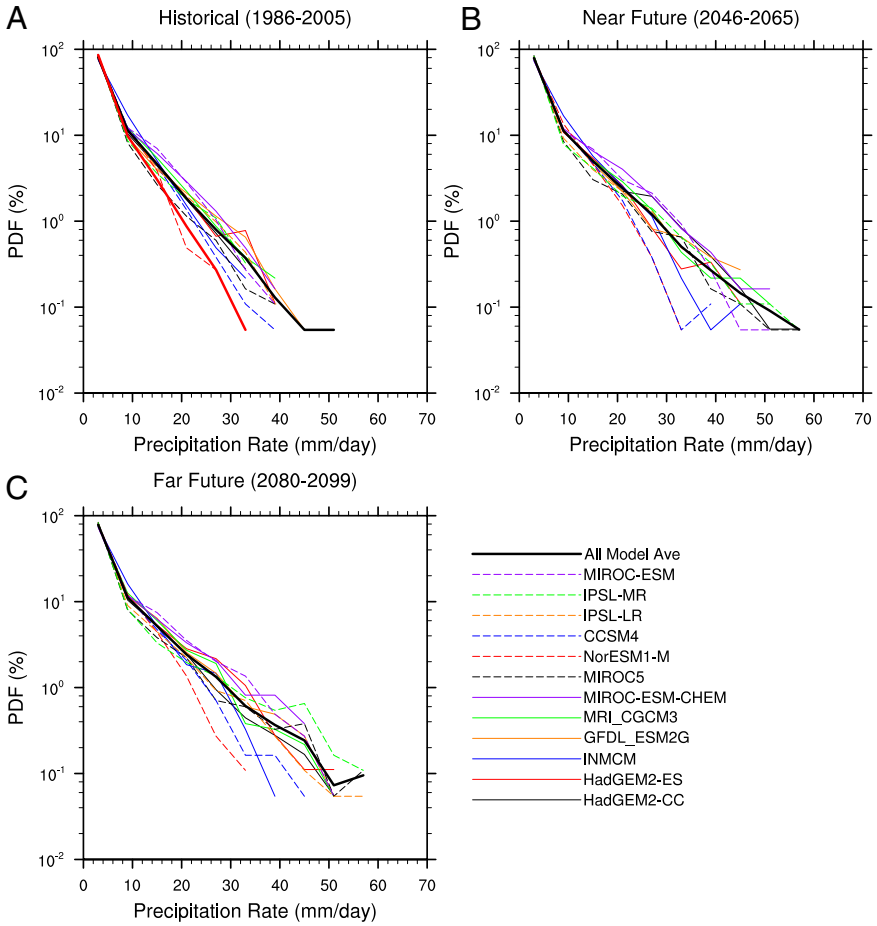

Fig. S9. Probability distribution functions of daily precipitation (millimeters day^{-1}) for three time periods: (*A*) historical (1986–2005) for CPC observations (thick red line), 12 individual model members (thin colored lines), and the present-day multimodel average (thick black line); (*B*) the near future (2046–2065) RCP8.5 Assessment Report 5 (AR5) individual simulations (thin colored lines) and 12-model average (thick black line); and (*C*) the far future (2080–2099) RCP8.5 AR5 individual model simulations (thin colored lines) and 12-model average (thick black line).

Table S1. Risk factors for dissolved phosphorus loss from agriculture

Risk factor	Trend	Basis of knowledge of trend	Impact on nutrient loading	Mechanism
Fall fertilizer application rather than spring	+	Impact documented by Ohio Lake Erie Phosphorus Task Force (1); trend documented in neighboring regions (2) and anecdotally confirmed by farmers and certified crop advisors.	++	Longer exposure to precipitation.
Fertilizer broadcast on surface instead of injected or incorporated	+	Anecdotal (based on discussions with farmers and certified crop advisors).	++	More direct exposure to precipitation, lack of binding to soil particles.
Conservation tillage	+ (primarily pre-2000)	Data from Conservation Tillage Information Center, Purdue University.	+	Contribution to phosphorus stratification; incentive to surface-apply nutrients.
			–	Enhanced flow through soil matrix and reduced preferential flow lead to better contact with phosphorus-adsorption sites; enhanced water retention capacity.
Stratification of P in soil	+	Presence documented by NCWQR, trend inferred from conservation tillage trend. Eckert and Johnson (3) showed that stratification sets up quickly (3 y) without inversion tillage.	++	Surface application; breakdown of crop residue; lack of inversion tillage leads to phosphorus concentration near soil surface where leaching is most active.
Extent and efficiency of tile drainage	+	Research of Kevin King, USDA–ARS, The Ohio State University (Columbus, OH); Jane Frankenburg, USDA–NRCS, Purdue University (W. Lafayette, IN).	+	Decrease contact time between phosphorus and soil matrix.
Excessive fertilizer sales	Unknown	Practice documented (4), trend unknown.	+	More fertilizer, more export.
Consolidation of farms	+	Data from Census of Agriculture via National Agricultural Statistics Service.	+	Need for greater efficiency promotes surface application of fertilizers in the fall.
Animal numbers	+	Data from Census of Agriculture via National Agricultural Statistics Service.	+	More nutrients from manure.
Soil phosphorus concentrations	–	Data obtained by NCWQR from major soil-testing laboratories in Ohio (4).	–	Higher soil concentrations correlated with higher losses in runoff.

Impact of factors is based on consensus judgment of personnel involved with agriculture in northwest Ohio (USDA Natural Resources Conservation Service; USDA Agricutural Research Service; Ohio Department of Agriculture; certified crop advisors; The Andersons Inc., Toledo, Ohio; Tom Bruulsema, International Plant Nutrition Institute, Guelph, Ontario, Canada; NCWQR staff). For trend, + indicates an increase and – indicates a decrease. For impact, + indicates an increase in potential for nutrient loading, ++ indicates a large increase, and – indicates a decrease.

1. Strickland T, Fisher L, Korleski C (2010) Ohio Lake Erie Phosphorus Task Force Final Report (Ohio Environmental Protection Agency, Columbus, OH).
2. Napier T & Bridges T (2002) Adoption of conservation production systems in two Ohio watersheds: A comparative study. *J Soil Water Conserv* 57(4):229–235.
3. Eckert DJ, Johnson JW (1985) Phosphorus fertilization in no-tillage corn production. *Agron J* 77(5):789–792.
4. Mullen RW, Dayton EA (2010) Analysis of Soil Testing Laboratories and Data Mining. Final Report - Lake Erie Protection Fund Project TG02-09. Available at http://lakeerie.ohio.gov/LakeErieProtectionFund/FinalReports.aspx Last accessed March 14, 2013.

Table S2. Results of discharge and nutrient loading trend analyses, 1995–2011

	Simple regression			
Parameter	Trend, yr^{-1}	% change over 1995–2011	*P* value	Complex regression *P* value
Discharge, 10^6 m^3	9.72	42	0.12	—
TP load, Mg of P	5.01	58	0.14	0.56
PP load, Mg of P	2.28	31	0.39	0.003
DRP load, Mg of P	2.48	218	0.0004	<0.0001
TP DWMC, mg/L of P	4.73×10^{-4}	2.7	0.82	0.56
PP DWMC, mg/L of P	-2.36×10^{-3}	−16	0.16	0.003
DRP DWMC, mg/L of P	2.58×10^{-3}	98	<0.0001	<0.0001

Simple regression refers to regression against time only, complex regression refers to regression of logged parameter against ln (discharge), time, and sinusoidal seasonality factors. DWMC, discharge-weighted mean concentration (load/discharge).

Table S3. CMIP AR5 models used in present-day and future climate precipitation analysis

Model name	Institute	Resolution	Lat/Lon Eqv.
CCSM4	RSMAS	288 × 192	1.25° × 1°
GFDL-ESM2G	NOAA GFDL	144 × 90	2.5° × 2°
HadGEM2-CC	MOHC	192 × 145	1.875° × 1.25°
HadGEM2-ES	MOHC	192 × 145	1.875° × 1.25°
INMCM4	INM	180 × 120	2° × 1.5°
IPSL-CM5-LR	IPSL	96 × 96	3.75° × 1.875°
IPSL-CM5-MR	IPSL	144 × 143	2.5° × 1.25°
MIROC-ESM	MIROC	256 × 128	1.4° × 1.4°
MIROC-ESM-Chem	MIROC	128 × 64	2.8° × 2.8°
MIROC5	MIROC	256 × 128	1.4° × 1.4°
MRI-CGCM3	MRI	320 × 160	1.25° × 1.125°
NorESM	NCC	144 × 96	2.5° × 1.875°

CCSM, Community Climate System Model; ESM, Earth System Model; HadGEM, Hadley Centre Global Environment Model; INM, Institute for Numerical Mathematics; INMCM, INM Climate Model; IPSL, Institut Pierre-Simon Laplace; MIROC, Model for Interdisciplinary Research on Climate Japan Agency for Marine-Earth Science and Technology; MOHC, Met Office Hadley Centre; MRI, Meteorological Research Institute; MRI-CGCM, MRI Coupled ocean-atmosphere General Circulation Model; NCC, Norwegian Climate Center; NOAA GFDL, National Oceanic and Atmospheric Administration Geophysical Fluid Dynamics Laboratory; NorESM, Norwegian Earth System Model; RSMAS, Rosenstiel School of Marine and Atmospheric Science, University of Miami.